THE JOURNAL OF BIOLOGICAL CHEMISTRY VOL. 288, NO. 31, pp. 22745–22757, August 2, 2013

Solution NMR Analyses of the C-type Carbohydrate Recognition Domain of DC-SIGNR Protein Reveal Different Binding Modes for HIV-derived Oligosaccharides and Smaller Glycan Fragments[S]

Received for publication, January 31, 2013, and in revised form, June 13, 2013 Published, JBC Papers in Press, June 20, 2013, DOI 10.1074/jbc.M113.458299

Fay Probert[‡1], **Sara B.-M. Whittaker**[§], **Max Crispin**[¶2], **Daniel A. Mitchell**[‖], **and Ann M. Dixon**[**3]

From the [‡]*Molecular Organisation and Assembly in Cells Doctoral Training Centre,* [‖]*Warwick Medical School, and* ***Department of Chemistry, University of Warwick, Coventry CV4 7AL, United Kingdom, the* [§]*Henry Wellcome Building for Biomolecular NMR Spectroscopy, Birmingham Cancer Research UK Centre, School of Cancer Sciences, University of Birmingham, Vincent Drive, Edgbaston, Birmingham B15 2TT, United Kingdom, and the* [¶]*Oxford Glycobiology Institute, Department of Biochemistry, University of Oxford, South Parks Road, Oxford OX1 3QU, United Kingdom*

Background: DC-SIGNR, a C-type lectin that promotes infection of pathogens such as HIV, is a promising drug target.
Results: The carbohydrate recognition domain of DC-SIGNR is highly dynamic, displaying unique binding modes for individual glycans.
Conclusion: More complex, disease-associated glycans have binding modes different from those of smaller glycans previously studied.
Significance: Understanding ligand-binding properties and solution dynamics of DC-SIGNR will facilitate therapeutic design.

The C-type lectin DC-SIGNR (dendritic cell-specific ICAM-3-grabbing non-integrin-related; also known as L-SIGN or CD299) is a promising drug target due to its ability to promote infection and/or within-host survival of several dangerous pathogens (*e.g.* HIV and severe acute respiratory syndrome coronavirus (SARS)) via interactions with their surface glycans. Crystallography has provided excellent insight into the mechanism by which DC-SIGNR interacts with small glycans, such as $(GlcNAc)_2Man_3$; however, direct observation of complexes with larger, physiological oligosaccharides, such as $Man_9GlcNAc_2$, remains elusive. We have utilized solution-state nuclear magnetic resonance spectroscopy to investigate DC-SIGNR binding and herein report the first backbone assignment of its active, calcium-bound carbohydrate recognition domain. Direct interactions with the small sugar fragments Man_3, Man_5, and $(GlcNAc)_2Man_3$ were investigated alongside $Man_9GlcNAc$ derived from recombinant gp120 (present on the HIV viral envelope), providing the first structural data for DC-SIGNR in complex with a virus-associated ligand, and unique binding modes were observed for each glycan. In particular, our data show that DC-SIGNR has a different binding mode for glycans on the HIV viral envelope compared with the smaller glycans previously observed in the crystalline state. This suggests that using the binding mode of $Man_9GlcNAc$, instead of those of small glycans, may provide a platform for the design of DC-SIGNR inhibitors selective for high mannose glycans (like those on HIV). ^{15}N relaxation measurements provided the first information on the dynamics of the carbohydrate recognition domain, demonstrating that it is a highly flexible domain that undergoes ligand-induced conformational and dynamic changes that may explain the ability of DC-SIGNR to accommodate a range of glycans on viral surfaces.

Calcium-dependent carbohydrate-binding proteins of the C-type lectin family play a large role in the mammalian immune system (1) and have been shown to be responsible for pathogen recognition and neutralization, cell-cell adhesion, and receptor-mediated endocytosis (2). C-type lectins recognize glycan structures with high selectivity via calcium-dependent carbohydrate recognition domains (CRDs)[4] (3). The C-type lectin DC-SIGNR (dendritic cell-specific ICAM-3-grabbing non-integrin-related; also known as L-SIGN or CD299) is a type II transmembrane protein that recognizes high mannose *N*-linked oligosaccharides on viral envelopes and host glycoproteins (4). Although DC-SIGNR is known to bind high mannose ligands, little is known about this molecule's biological function, partly due to difficulties studying its specialized and often inaccessible cell types in which it is natively expressed. Furthermore, functional orthologues of DC-SIGNR in model species such as mice are not clear cut, thus restricting the value and meaning of gene-targeting studies, such as knock-out animals. In humans, it is expressed on specialized endothelia found in

[S] This article contains supplemental Tables S1 and S2 and Figs. S1–S7.
The chemical shifts and ^{15}N relaxation data have been deposited in the BioMagnetic Resonance Bank under BMRB accession number 19297 (www.bmrb.wisc.edu/).

[1] Recipient of a studentship from the Engineering and Physical Sciences Research Council through the Molecular Organisation and Assembly in Cells Doctoral Training Centre.
[2] Supported by the International AIDS Vaccine Initiative and the Center for HIV/AIDS Vaccine Immunology and Immunogen Discovery.
[3] To whom correspondence should be addressed: Dept. of Chemistry, University of Warwick, Coventry CV4 7AL, United Kingdom. Tel.: 44-2476-150037; Fax: 44-2476-524112; E-mail: ann.dixon@warwick.ac.uk.

[4] The abbreviations used are: CRD, carbohydrate recognition domain; SARS, severe acute respiratory syndrome coronavirus; HSQC, heteronuclear single quantum correlation.

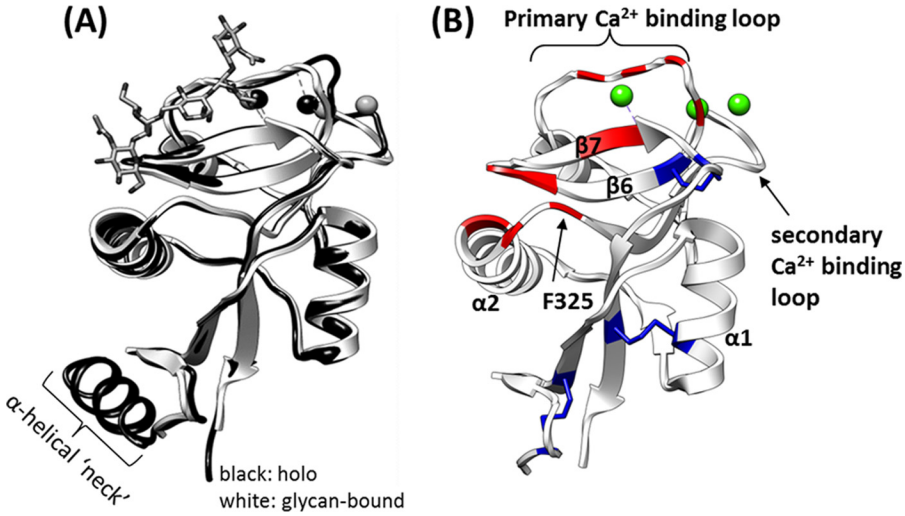

FIGURE 1. **Insight from current crystal structures.** *A*, comparison of holo-structure (Protein Data Bank code 1XPH; *black*) and $(GlcNAc)_2Man_3$-bound (1K9J; *white*) crystal structure. Ca^{2+} ions are represented by *spheres*. All published crystal structures adopt nearly identical conformations, suggesting that the DC-SIGNR CRD adopts the same conformation during crystal formation with or without glycan. *B*, residues that form direct contacts/bonds with the glycan in the structure of the $(GlcNAc)_2Man_3$·CDR complex (1K9J; ligand not shown) are highlighted in *red*, disulfide bonds are shown in *blue*, and bound calcium ions are shown in *green*.

liver sinusoids, lymph nodes, and placental capillaries, suggesting important roles in leukocyte adhesion and migration (5). Expression has also been found on precursor lung epithelial cells (6), a site where there is potential exposure to airborne viruses. Despite the lack of understanding of its biological function, important disease associations have been reported for DC-SIGNR, such as vertical transmission of human immunodeficiency virus (HIV) (7) and severe acute respiratory syndrome coronavirus (SARS) infection (8). Recent work also indicates involvement of DC-SIGNR in respiratory syncytial virus infection (9), influenza (10), and within-host dynamics of Dengue infection (11). The affinity of DC-SIGNR for glycoproteins on the surface of viruses, as well as its localization at the primary sites of virus replication, promotes in *trans* infection by viruses, such as HIV. Specifically, DC-SIGNR is believed to promote HIV infection by transferring the virus to adjacent $CD4^+$ T-cells, where the HIV glycoprotein gp120 binds to the CD4 receptor on these cells, promoting entry of the virus into host T-cells. This reinforces the important role of this protein in immunity as well as its considerable potential as a drug target.

Therapeutic strategies designed to inhibit or stimulate the function of C-type lectins, such as DC-SIGNR, are scarce, considering the scale of the diseases involved in their biology. Of particular interest is the interaction of the DC-SIGNR CRD (residues 262–400) with $Man_9GlcNAc_2$, one of the dominant oligosaccharides present on the HIV envelope glycoprotein gp120. It has been speculated that direct blockade of DC-SIGNR could provide a topical barrier against primary HIV infection. Therefore, a detailed understanding of the interaction between the DC-SIGNR CRD and the oligosaccharides present on viral glycoproteins is valuable for the design of compounds that could act as antiviral drugs.

Thus far, x-ray crystallography has been the primary method employed for atomic level study of the DC-SIGNR CRD structure. To date, four crystal structures have been deposited for the DC-SIGNR CRD: 1) in complex with the branched pentasaccharide $(GlcNAc)_2Man_3$ (Protein Data Bank code 1K9J); 2) in the absence of ligand (but with one Ca^{2+}) and containing a portion of the N-terminal α-helical neck region (1XPH); 3) with two repeats of the α-helical neck region and one sodium ion bound (1XAR); and 4) in complex with Lewis-x trisaccharide and containing a portion of the neck (1SL6). The DC-SIGNR CRD adopts a typical "lectin fold" consisting of α-helices and antiparallel β-sheets connected by irregular loops that are stabilized by disulfide bonds and calcium ions (2). The structure of the DC-SIGNR CRD in complex with $(GlcNAc)_2Man_3$ provides insight into the CRD structure and potential ligand binding mechanism, notably revealing that an extended binding site exists that is composed of α-helix 2 and a solvent-exposed Phe-325 residue. The C-terminal end of α-helix 2 packs against the loop joining β-sheets 6 and 7, forming a continuous binding surface (see Fig. 1*A*). The "shelf" formed by α-helix 2 and Phe-325 creates a shape complementary to the Manα1–6Man moiety that forms van der Waals contacts with Phe-325 and hydrogen-bonds with Ser-372. The Phe-325 residue is also thought to be responsible for the selective binding of DC-SIGNR to the outer branched trimannose moiety of high mannose structures (such as $Man_9GlcNAc_2$) because it sterically hinders binding to the inner branched mannose (4).

In addition, coordination bonds via the primary Ca^{2+} binding loop (residues 356–364) and contacts with residues in β-sheets 6 and 7 have been described (4). Regions of interest that form contacts with $(GlcNAc)_2Man_3$ are shown in Fig. 1*B* and listed in supplemental Table S1. However, crystal structures of the DC-SIGNR CRD bound to larger, physiologically relevant oligosaccharides, such as $Man_9GlcNAc_2$, have proved to be unattainable thus far. This may be due to as yet uncharacterized conformational/dynamic factors that prohibit crystal growth and diffraction.

High field nuclear magnetic resonance (NMR) studies of the DC-SIGNR CRD have not been reported previously, although NMR studies of ligand interactions with the homologous pro-

tein DC-SIGN have started to emerge (12–18). These largely ligand-based studies have been similarly restricted to the use of small glycans and sugar mimetics and have not approached conformational or dynamic properties of DC-SIGN in solution or included larger physiological glycans such as $Man_9GlcNAc_2$. As a result, binding of disease-associated ligands such as $Man_9GlcNAc_2$ to molecules such as DC-SIGNR and DC-SIGN has been assumed to be consistent with the binding modes observed for smaller glycan fragments co-complexed in the crystalline state (19, 20).

We aimed to increase current understanding of DC-SIGNR-glycan interactions by investigating the binding of the DC-SIGNR CRD to a number of oligosaccharides in solution using heteronuclear solution state NMR techniques that can better deal with issues of dynamics that we surmise to be restricting the rate of progress in DC-SIGNR crystallography. Here we present the backbone assignment of the DC-SIGNR CRD as well as the first structural data for binding of a disease-associated ligand, namely $Man_9GlcNAc$. These results are extended using dynamics measurements (^{15}N T_1 and T_2), which suggest that the same regions of the DC-SIGNR CRD are highly dynamic in both holo-form and ligand-bound form and interconvert between a number of conformations at similar rates. Our results support the location of the extended binding site observed in the crystal structure of DC-SIGNR CRD-$(GlcNAc)_2Man_3$ complex (1K9J). However, our data also demonstrate that DC-SIGNR employs a different binding mode for $Man_9GlcNAc$, suggesting that DC-SIGNR may interact with the HIV glycoprotein gp120 in a way different from that previously observed for smaller glycans. Dynamics data provide new information on the flexible nature of DC-SIGNR and highlight new regions of the protein that are potentially important for ligand recognition.

EXPERIMENTAL PROCEDURES

Expression and Purification of $^{13}C/^{15}N$ Isotopically Labeled DC-SIGNR CRD—The pT5T overexpression plasmids containing modified cDNA inserts encoding the human DC-SIGNR CRD sequence (Q9H2X3 (CLC4M_HUMAN; residues 262–400); cDNA provided by Elizabeth Soilleux, University of Oxford) were prepared as described previously (21) and subjected to DNA sequencing in order to confirm sequence integrity. The plasmids were then used to transform *Escherichia coli* strain BL21(DE3), and frozen bacterial stocks were prepared in 15% glycerol and stored at −80 °C. Protein expression was carried out in M9 minimal medium (22) (pH 7.3) containing 50 μg/ml ampicillin, 1 g of [^{15}N]ammonium chloride, and 2 g of [^{13}C]glucose per liter of culture. Two 100-ml starter cultures were inoculated using colonies from an M9/ampicillin plate. Starter cultures were grown at 37 °C with shaking at 200 rpm for 24 h before dilution into 1 liter of M9 minimal medium to a starting $A_{600\,nm}$ of ~0.2. Once an $A_{600\,nm} = 0.7$ was reached, the 1-liter culture was induced with isopropyl-β-D-thiogalactoside to a final concentration of 350 μM. Refolding of the CRD from inclusion bodies was performed as described (21). The protein CRD fragment was purified using a 2-ml mannose-Sepharose column (kindly provided by Dr. Russell Wallis, University of Leicester) equilibrated with 25 mM HEPES, 5 mM $CaCl_2$, 150 mM NaCl, pH 7.8 (loading buffer) as described (21). Protein purity and oligomeric state were assessed using mass spectrometry, SDS-PAGE, and circular dichroism (CD) spectroscopy. The protein predominantly migrated near its monomeric molecular mass of 17.1 kDa (for the isotopically labeled protein) and yielded a CD spectrum that is in good agreement with previous reports (21).

Carbohydrates—All carbohydrate fragments ($(GlcNAc)_2Man_3$ (M592), Man_3 (M336), Man_5 (M536)) were purchased from Dextra Laboratories (Reading, UK). The $Man_9GlcNAc$ was prepared by digestion of recombinant gp120 with endoglycosidase H using gp120 glycoprotein harvested from 10 μM kifunensine-treated HEK 293T cultures as described (23). The gp120 glycoform was characterized by mass spectrometry as shown in supplemental Fig. S1.

NMR—Purified protein samples were subjected to extensive dialysis into water (1 week with 12 buffer changes) before lyophilization. The protein was then dissolved in 180 μl of 20 mM deuterated HEPES-d_{18}, 20 mM NaCl, pH 6.8, in 10% D_2O, 90% H_2O to a final concentration of 0.7 mM DC-SIGNR CRD. NMR experiments were carried out at 37 °C on either a 700-MHz Bruker Avance spectrometer fitted with cryoprobe (University of Warwick) or a 5-mm triple resonance cold probe-equipped Varian Unity Inova 800-MHz spectrometer (Henry Wellcome Building for Biomolecular NMR Spectroscopy, University of Birmingham). Proton chemical shifts were referenced against external DSS, whereas nitrogen chemical shifts were referenced indirectly to DSS using the absolute frequency ratio (24). One-dimensional proton spectra were acquired using the pulse sequence described by Liu *et al.* (25). Two-dimensional ^1H–^{15}N HSQC spectra (26) were recorded with 128 increments in the t_1 domain and 1024 data points in the t_2 dimension. The sweep width was 18.0 ppm in the ^1H dimension and 31.8 ppm in the ^{15}N dimension. The triple resonance (^1H-^{13}C-^{15}N) experiments (CBCA(CO)NH (27), CBCANH (28), HNCA (29), HN(CO)CA (30), HNCO (29), and HN(CA)CO (31)) were recorded with 128 increments in the t_1 domain, 40 increments in the t_2 domain, and 2048 increments in the t_3 domain. Spectra were processed using Topspin version 2.0 (unless otherwise stated) and analyzed using CCPN Analysis software version 2.1.5 (32, 33) and SPARKY version 3 (34). Secondary structure predictions based on the chemical shift index were carried out using TALOS+ (35).

Unlabeling of specific residues, by the addition of 100 mg of unlabeled amino acid to double-labeled M9 medium, was used to assign difficult residues (such as the highly mobile residues Asn-102 and Asn-103 in the primary calcium binding loop).

Carbohydrate Titrations—Titration experiments were carried out by adding increasing amounts of carbohydrate (0.2, 0.5, 1.0, 2.0, 5.0, 10.0, and 20.0 mM Man_3; 1.0, 2.0, 5.0, and 10.0 mM Man_5 and $(GlcNAc)_2Man_3$; and 0.1, 0.3, 0.7, 1.0, 1.5, 2.0, 5.0, and 10.0 mM $Man_9GlcNAc$) to 0.7 mM [U-^{15}N,^{13}C]DC-SIGNR CRD at pH 6.8 and acquiring a series of two-dimensional ^1H-^{15}N HSQC spectra at 37 °C. The pH and temperature were held constant throughout the experiments. The three sugar fragments reached saturation by 10 mM, whereas relaxation properties prevented the determination of $Man_9GlcNAc$ saturation.

The total chemical shift perturbation per residue ($\Delta\delta_{total}$) was calculated using Equation 1,

$$\Delta\delta_{total} = \sqrt{(\Delta\delta_{NH})^2 + (0.1\Delta\delta_N)^2} \quad \text{(Eq. 1)}$$

where $\Delta\delta_{NH}$ and $\Delta\delta_N$ represent the chemical shift differences in the ^1H and ^{15}N dimensions, respectively. The weighting factor of 0.1 applied to the nitrogen chemical shift corresponds to the difference in magnetogyric ratios of ^{15}N with ^1H nuclei. Although a weighting factor of 0.15 can also be used, Schumann *et al.* (36) found little difference between the two weighting factors and concluded that either is sufficient. Residues significantly perturbed by the ligand addition were determined by calculating the S.D. of the chemical shift perturbations across all residues for each carbohydrate and using this as a cut-off (36).

To determine the disassociation constant (K_D), titration curves were fit to Equation 2, valid for 1:1 complex formation in fast exchange on the NMR chemical shift time scale,

$$\Delta\delta_{(total,x)} = \Delta\delta_{max}\frac{(K_D + x + [P]) - \sqrt{(K_D + x + [P])^2 - (4[P]x)}}{2[P]} \quad \text{(Eq. 2)}$$

where x and $[P]$ represent the ligand and protein concentration, respectively; $\Delta\delta_{(total,\,x)}$ is the total chemical shift perturbation at ligand concentration x, and $\Delta\delta_{max}$ is the total chemical shift perturbation at saturation of ligand (37, 38). The fit was carried out and analyzed in Origin version 8.5 using the non-linear least squares method.

Backbone Dynamics—^{15}N longitudinal (T_1) and transverse (T_2) relaxation times were measured using the procedures of Kay *et al.* (39) and Farrow *et al.* (40). For T_1 measurements, 11 spectra were recorded with relaxation delays between 0.01 and 0.750 s. Matrices of 1024 × 128 complex data points were acquired, using 32 scans per t_1 increment and a recycle delay of 3 s. For T_2 measurements, 10 spectra were recorded with relaxation delays of 0.0077–0.0850 s. Matrices of 1024 × 128 complex data points were recorded, using 32 (holoprotein) or 64 (Man_5-bound protein) scans per t_1 increment and a recycle delay of 3 s. Sample heating due to cold probe sensitivity was compensated for by application of continuous wave irradiation to ^{15}N nuclei for a variable time period during the recycle delay (41). Spectral widths of 13,008.1 Hz (^1H) and 2500 Hz (^{15}N) were measured. Relaxation data were acquired in an interleaved manner to minimize the effects of sample heating, and three repeat measurements for each of the T_1 and T_2 data sets were made for determination of peak height uncertainties. Relaxation spectra were processed in NMRpipe (42), and peak heights were calculated and fit to a monoexponential decay in SPARKY 3 (34).

RESULTS

Assignment of Ca^{2+}-bound DC-SIGNR CRD—To investigate the structure, dynamics, and ligand-binding modes of the human DC-SIGNR CRD domain in solution, solution state NMR was used. A 0.7 mM sample of the recombinant 138-residue fragment (containing CRD residues 262–399) was prepared with uniform $^{13}C/^{15}N$ labeling in the presence of 4 mM Ca^{2+} (pH 6.8). The purity, secondary structure, and oligomeric state were probed using SDS-PAGE, mass spectrometry, and circular dichroism, and in all cases, we observed pure, monomeric protein. Purification of the CRD using a mannose-Sepharose column served as an effective screen for correct and functional folding of the CRD because incorrectly folded protein fails to bind to immobilized mannose on the column and elutes much earlier.

The ^1H-^{15}N HSQC spectrum of the calcium-bound DC-SIGNR CRD is shown in Fig. 2, and the sequential assignment of the N, C, and H nuclei along the protein backbone was achieved using a full suite of triple resonance experiments (see "Experimental Procedures"). The assignments are given in Fig. 2 and supplemental Table S2. Of the 138 amino acids in the CRD, 5 proline residues do not appear in the HSQC spectrum due to their lack of a backbone amide group, and 17 residues (8 at the N terminus and 9 at the C terminus) were also not present. Of the observable residues present in the HSQC, 96% have been unambiguously assigned (80% of the total CRD).

The C, H, and N chemical shift assignments (deposited at BMRB, ID 19297) facilitated determination of secondary structure using the TALOS+ program (35) to designate regions containing α-helical/β-sheet structure based on dihedral angle predictions. The secondary structure prediction is in good agreement with crystal data (Protein Data Bank code 1K9J) (supplemental Fig. S2). Therefore, we have used published crystal structures as a foundation for comparison of solution data in this work.

Binding Modes for Three Glycan Fragments in Complex with DC-SIGNR CRD—The HSQC spectrum shown in Fig. 2 provides a "map" of the CRD in the calcium-bound state. To investigate a range of glycan-CRD interactions in solution, with an eye toward difficult-to-crystallize glycans, a series of HSQC spectra were acquired upon titration of the oligosaccharide fragment Man_3, Man_5, or $(GlcNAc)_2Man_3$ (see Fig. 3) into the DC-SIGNR CRD. Analysis of $(GlcNAc)_2Man_3$, the sugar present in the 1K9J structure, allowed the direct comparison of results in solution with published crystal data. As shown in Fig. 4 and supplemental Figs. S3–S5, binding of all three sugars resulted in significant chemical shift perturbations along the length of the CRD. The S.D. of the chemical shift perturbation across all residues (*dashed line* in Fig. 4) was used (36) to determine the residues most affected by binding. Perturbations above this threshold were considered significant and are mapped onto the $(GlcNAc)_2Man_3$-CRD structure (Protein Data Bank code 1K9J) as shown in Fig. 5.

Binding of all three sugar fragments was consistent with a principal glycan binding site composed of the primary Ca^{2+}-binding loop (residues 356–364), previously proposed to directly interact with the glycan (3, 4, 19, 20), and residues in β-sheets 6 and 7 at the core of the protein fold (residues 368–379; Fig. 1*B*).

However, binding of the glycan fragments was not universally consistent with the proposed "shelf" formed by α-helix 2 and Phe-325. The three glycan fragments show marked differences in the degree of perturbation of residues in α-helix 2 (residues 308–323), as shown by the *circle* in Fig. 5*A*. Only binding of $(GlcNAc)_2Man_3$, the glycan bound in the 1K9J structure, yielded appreciable chemical shift perturbations in α-he-

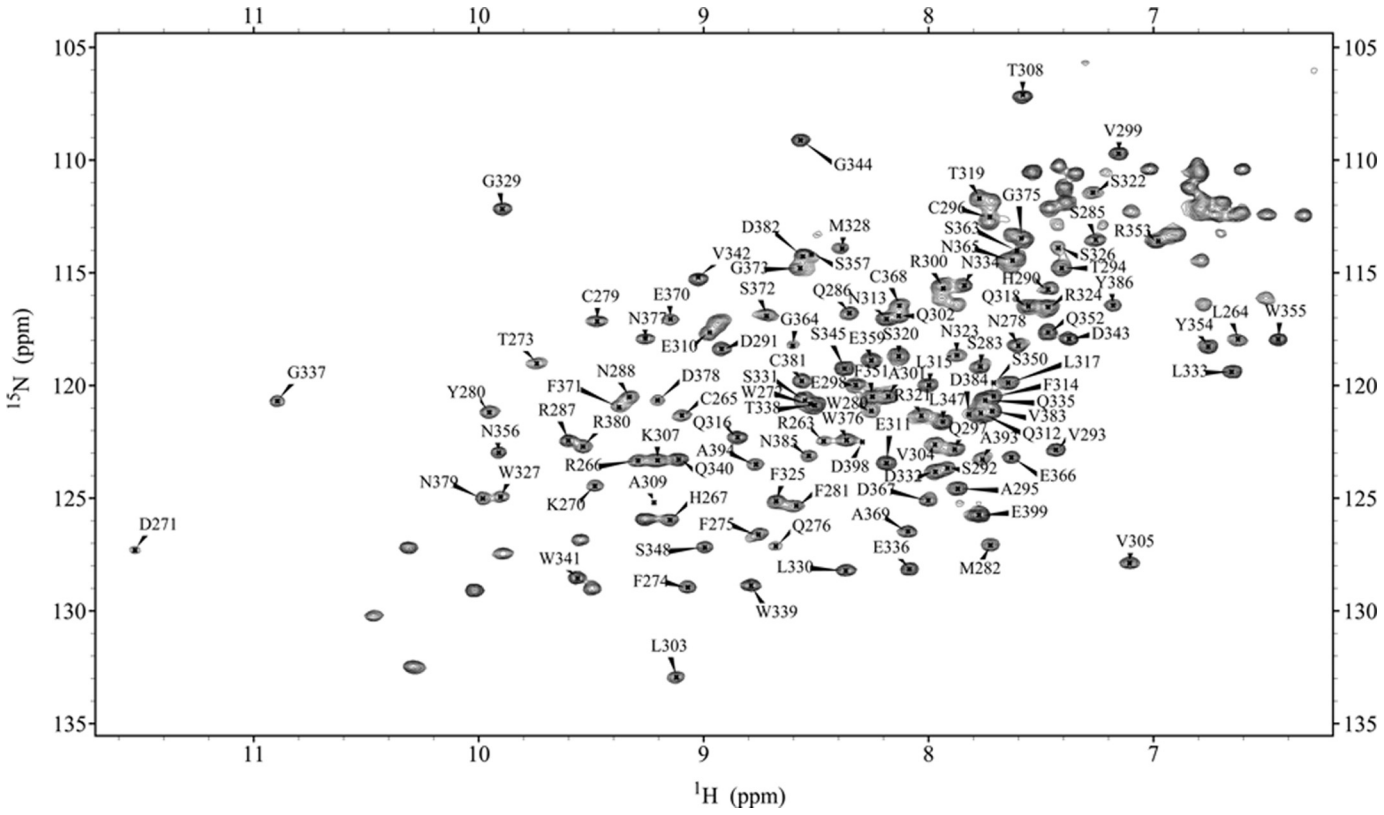

FIGURE 2. **Assignment of DC-SIGNR CRD.** Shown are the HSQC spectrum and annotated backbone assignment of holo-DC-SIGNR CRD (20 mM HEPES-d_{18}, 20 mM NaCl, 4 mM $CaCl_2$, pH 6.8, 37 °C), showing 96% of the observed ^{1}H, ^{15}N, and ^{13}C resonances assigned.

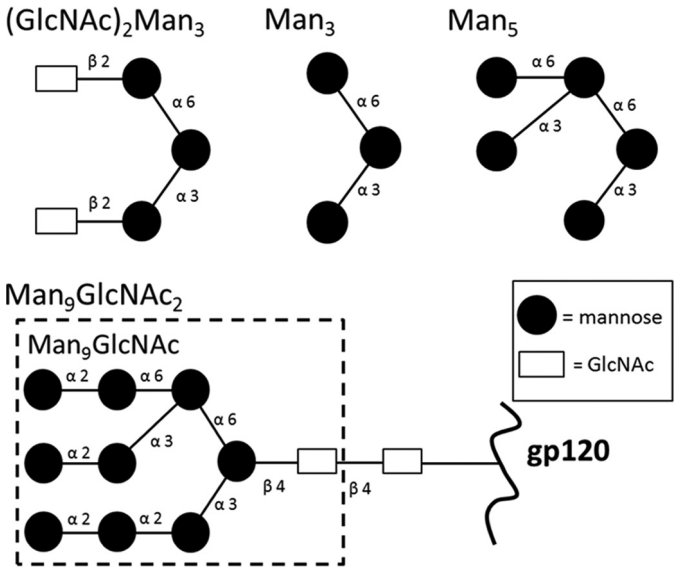

FIGURE 3. **Schematic representation of glycans used in this study.** Binding of all four glycans to the DC-SIGNR CRD was measured using chemical shift perturbation analyses.

lix 2 (specifically residues 314–324). Even then, the Phe-325 residue in α-helix 2 shown to form a direct contact with $(GlcNAc)_2Man_3$ in the crystal, was not perturbed significantly in solution. Even fewer perturbations in α-helix 2 were observed upon binding of Man_3 and Man_5, and neither sugar induced any perturbation of the Phe-325 peak. However, Man_3 and Man_5 binding significantly affect Ser-326, adjacent to Phe-325, whereas $(GlcNAc)_2Man_3$ binding does not.

The chemical shift perturbations observed here in solution also highlighted changes in additional regions of the CRD, distal to the proposed glycan binding site. Man_3 and Man_5 binding induced perturbation of residues 270 and 271 at the N terminus of the CRD (*solid box* in Fig. 5, *B* and *C*), whereas $(GlcNAc)_2Man_3$ binding exhibited unique perturbations in the loop region consisting of residues 382–385 (Fig. 5*A*, *dashed box*). This suggests that perturbations in this region may be due to the GlcNAc moieties, possibly in conjunction with their β-(1,4) linkages to the trimannose core. These residues were not highlighted in previous glycan-binding studies, suggesting that a conformational or dynamics change is taking place in this region.

More broadly, when our results are compared with the existing structural data, the number of chemical shifts affected by ligand binding in all cases is greater than was expected based on the size of the canonical binding site in the crystal (see summary in supplemental Table S1). This, along with the fact that there are chemical shift perturbations distal to the canonical glycan binding surface, suggests that significant changes in conformation and/or dynamics occur upon ligand binding in solution. This is in contrast to results obtained from crystallography, which yield virtually identical average structures for the free and ligand-bound states (4, 43) (see Fig. 1*A* for an overlay of two representative structures for these opposing states).

Binding of $Man_9GlcNAc$ Derived from HIV gp120 to the DC-SIGNR CRD—To extend current knowledge of the DC-SIGNR CRD to binding of more complex, physiologically important, and/or disease-associated ligands and provide a better understanding of DC-SIGNR-HIV interactions, similar titration

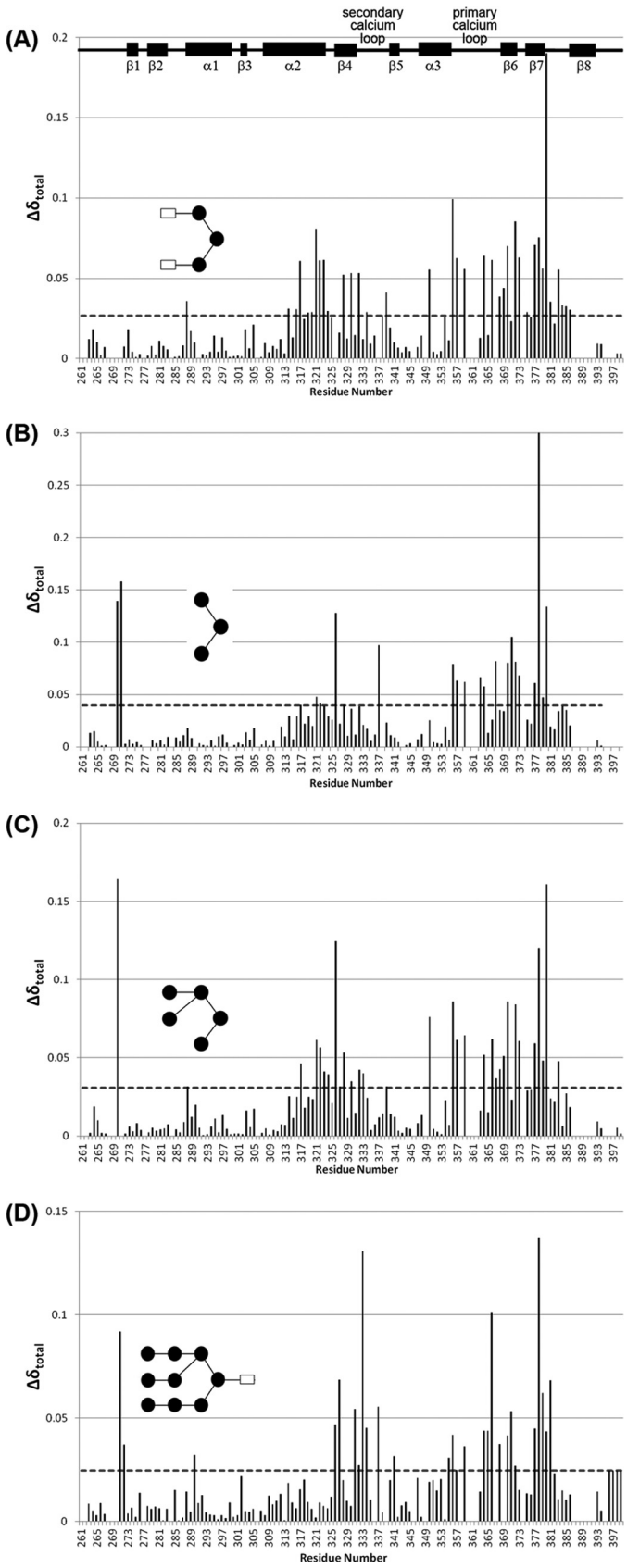

FIGURE 4. **Chemical shift perturbation upon ligand-binding.** Total chemical shift perturbation per residue upon the addition of $(GlcNAc)_2Man_3$ (*A*), Man_3 (*B*), Man_5 (*C*), and $Man_9GlcNAc$ (*D*) was calculated according to Equation 1. *Dashed horizontal lines* represent the 1 × S.D. cut-off used in each data set, above which a change was considered significant.

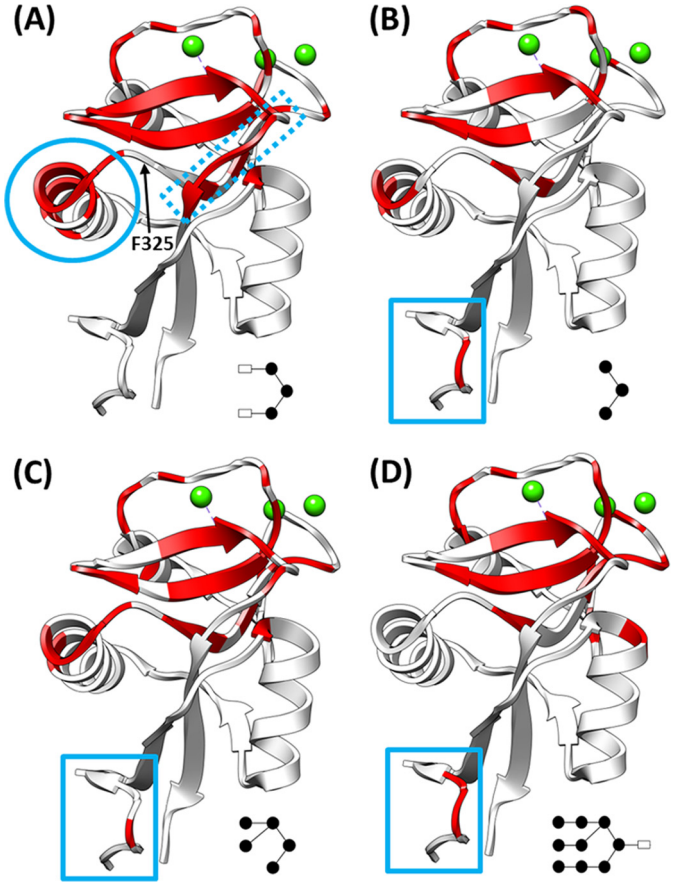

FIGURE 5. **Regions affected by glycan binding.** Chemical shifts with perturbations greater than 1 × S.D. upon the addition of 5 mM $(GlcNAc)_2Man_3$ (*A*), Man_3 (*B*), Man_5 (*C*), and $Man_9GlcNAc$ (*D*) are shown in *red* mapped onto the structure of the $(GlcNAc)_2Man_3$·CDR complex (Protein Data Bank code 1K9J). A schematic of the bound glycan is given in the *lower right corner* of each *panel*. These maps highlight the conserved binding regions as well as regions unique to each glycan.

experiments were carried out using $Man_9GlcNAc$ derived from the gp120 protein of HIV. $Man_9GlcNAc$ is very closely related to $Man_9GlcNAc_2$ on HIV gp120, differing by a single GlcNAc unit at the reducing terminus, which would be anchored to the polypeptide backbone and hence less likely to play a crucial role in DC-SIGNR binding (Fig. 3).

Similar to the glycan fragments, chemical shift perturbation data upon $Man_9GlcNAc$ binding (Figs. 4*D* and 5*D* and supplemental Fig. S6) is consistent with a principal binding site containing residues in β-sheets 6 and 7 and the primary calcium binding loop. The same effects on distal regions of the CRD (*e.g.* N-terminal residues 270–271; *solid box* in Fig. 5*D*) are also observed.

$Man_9GlcNAc$ binding results in no chemical shift changes for residues in the region thought to compose a "shelf" formed by α-helix 2 and Phe-325. This is interesting because all crystal structures (on small fragments of DC-SIGNR and the homologous protein DC-SIGN) highlight this shelf as forming part of the extended binding site. The NMR data presented here show that, in solution, α-helix 2 is involved in binding to $(GlcNAc)_2Man_3$ (and possibly to the smaller glycan fragments), which is in good agreement with 1K9J structure. However, α-helix 2 is not involved in binding to $Man_9GlcNAc$, suggesting that it has a mode of binding to the CRD different from that of $(GlcNAc)_2Man_3$ and that DC-SIGNR may interact with the

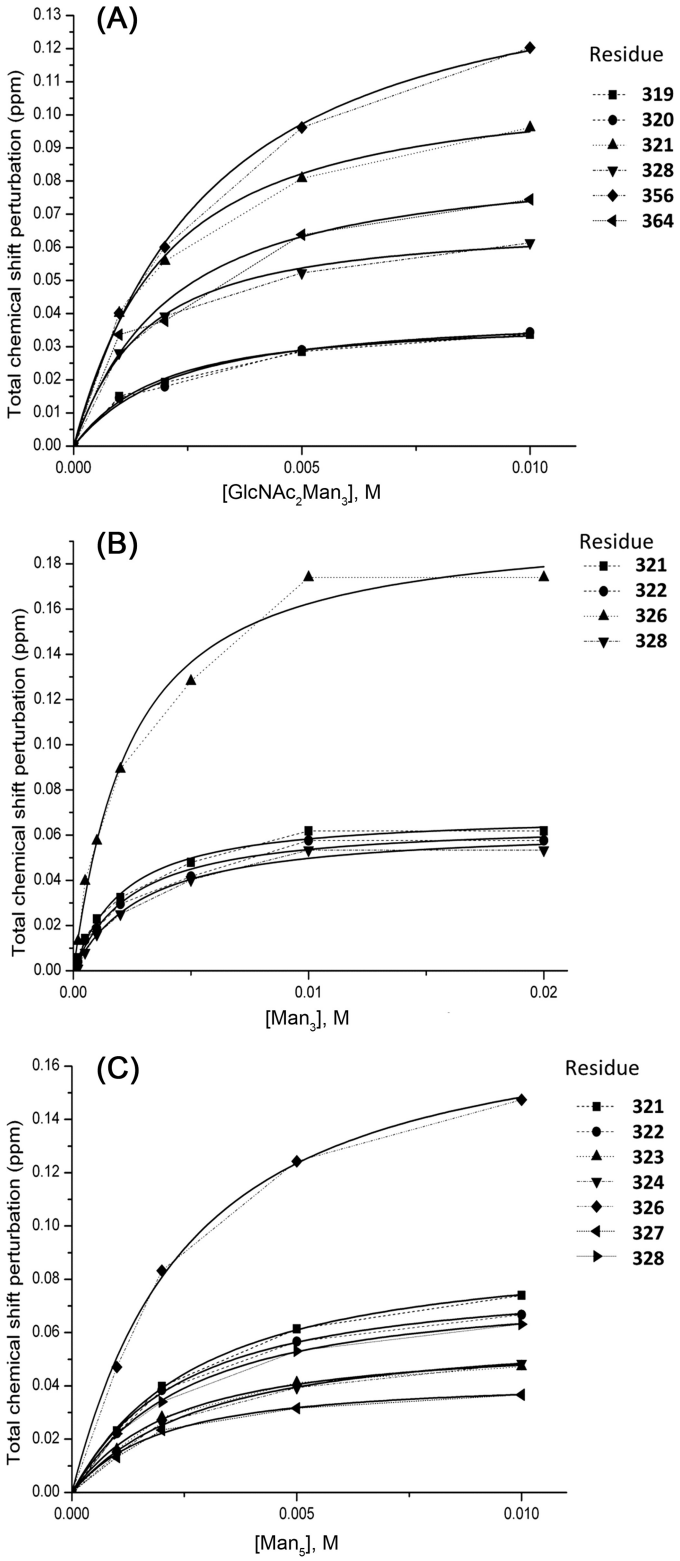

FIGURE 6. **Affinity of glycans for CRD.** Shown is a fit of chemical shift perturbations *versus* glycan concentration to a single site binding model for $(GlcNAc)_2Man_3$ (*A*), Man_3 (*B*), and Man_5 (*C*). Only data derived from residues near α-helix 2 are shown.

HIV glycoprotein gp120 in a way different from that observed in the$(GlcNAc)_2Man_3$-CRD complex. Ongoing work to determine a high resolution solution structure of DC-SIGNR CRD bound to this ligand will shed further light upon this.

TABLE 1
Dissociation constants calculated from chemical shift perturbations

Glycan	K_D
	mM
$(GlcNAc)_2Man_3$	1.57 ± 0.46
Man_3	2.04 ± 0.54
Man_5	2.20 ± 0.43

Ligand Binding Affinities in Solution—NMR titration data were also used to provide detailed affinity information. Supplemental Figs. S3–S5 show the HSQC spectra of the CRD acquired at increasing concentrations of $(GlcNAc)_2Man_3$, Man_3, or Man_5, respectively. The three sugar fragments behaved similarly upon titration, displaying linear chemical shift perturbations and no line broadening as ligand concentration was increased. This behavior is characteristic of fast exchange between free and bound protein on the NMR chemical shift time scale and suggests that the interaction between the CRD and sugar fragments is weak. This weak binding of our small sugar fragments is unsurprising in light of several reports that DC-SIGNR binds preferentially to larger, highly branched oligosaccharides (4, 19, 43). Fitting the chemical shift perturbations to a 1:1 binding model (see "Experimental Procedures"), which produced the best fits to the data, provides estimates of the dissociation constants for each sugar (Fig. 6). Table 1 shows that $(GlcNAc)_2Man_3$, Man_3, and Man_5 all bind with similar, weak affinities. K_D values ranged from 1.57 to 2.2 mM. This value is considerably weaker than binding of similar simple sugars to other lectin CRD domains, such as galectin-1 (lactose bound with a K_D of 40 μM (44) to 520 μM (45)), galectin-3 (lactose bound with a K_D of 231 μM (46)), BclA (methyl-α-D-mannoside bound with a K_D of 2.75 μM (47)), and the asialoglycoprotein receptor (binding constants of 66–539 μM were reported for a variety of simple sugars (48)). However, these K_D values are in line with the IC_{50} values of the analogous protein DC-SIGN for fucose (1.2 mM) and mannose (1.8 mM) (16).

Unlike the glycan fragments, binding of $Man_9GlcNAc$ caused substantial broadening and disappearance of a number of CRD peaks (supplemental Fig. S6), consistent with intermediate exchange on the NMR chemical shift time scale (49, 50). This suggests higher affinity binding of $Man_9GlcNAc$ compared with the sugar fragments (because we move from fast exchange to intermediate exchange as the lifetime of a complex is increased) and supports previous studies reporting a K_i value of 200 μM (21) for the DC-SIGNR·$Man_9GlcNAc_2$ complex. Studies of other lectins (*e.g.* galectin-1) also report increased affinity for larger, more complex glycans (45). However, due to the severe line broadening at the highest $Man_9GlcNAc$ concentrations (5 mM), an accurate K_D could not be estimated using NMR under these conditions.

NMR Dynamics—The high degree of dynamics in the DC-SIGNR CRD was first suspected after measurement of the HSQC spectrum of the Ca^{2+}-free (apo) form (supplemental Fig. S7), in which variable signal intensities prevented further study using three-dimensional NMR methods. Weak or missing signals suggest that, in its Ca^{2+}-free form, the protein can exchange between an ensemble of conformational states with a rate corresponding to the intermediate exchange regime on the NMR chemical shift time scale. The addition of Ca^{2+} to the

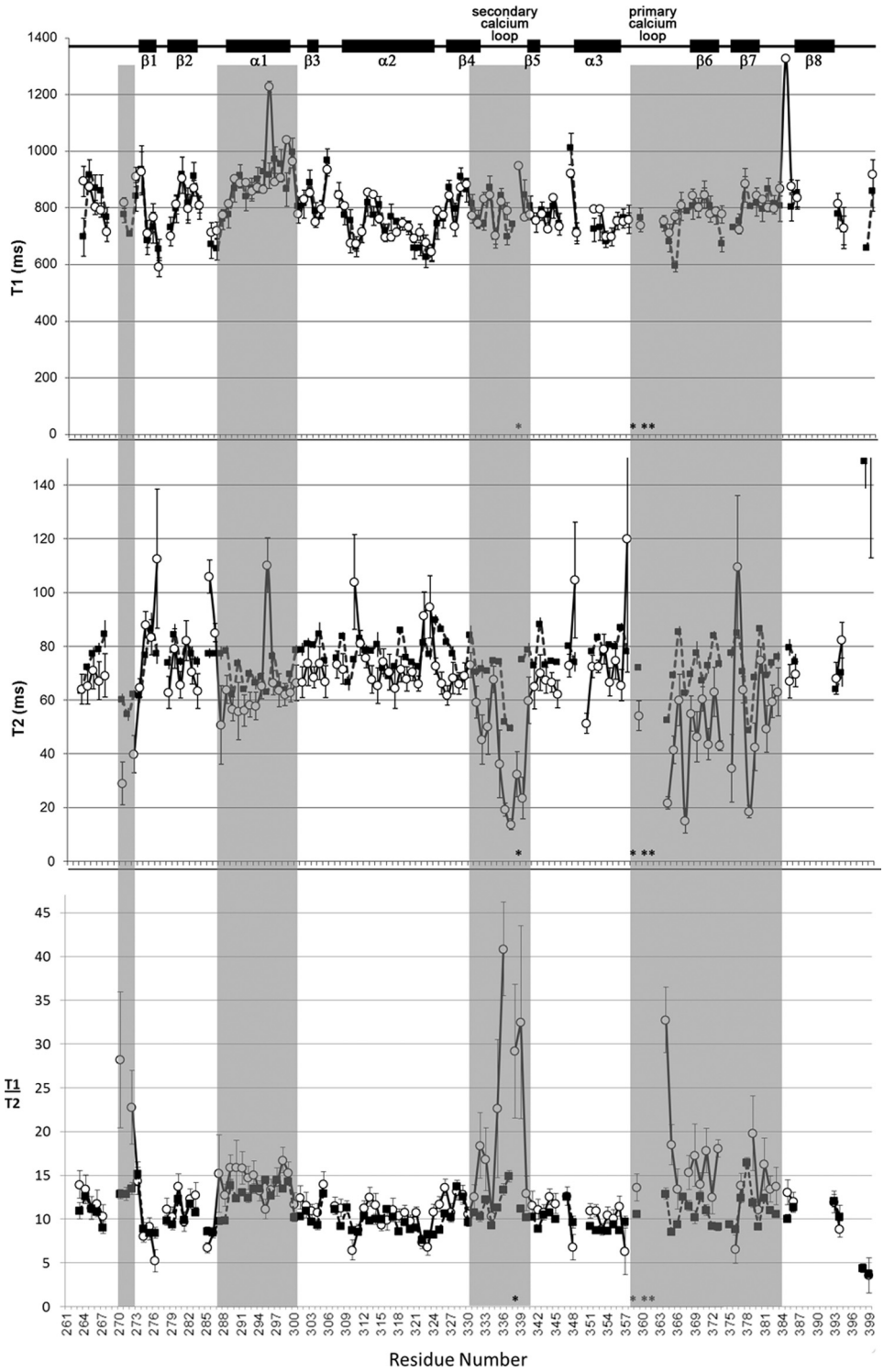

FIGURE 7. **Dynamics of the CRD.** Shown is a plot of per residue values for ^{15}N T_1 (*top*), ^{15}N T_2 (*middle*), and ^{15}N T_1/T_2 (*bottom*) for holo-DC-SIGNR CRD (*solid squares*) and Man_5-bound (*open circles*) DC-SIGNR CRD. *Asterisks* along the *bottom* of each *panel* denote residues that are not observed due to fast relaxation or exchange.

CRD improved the spectrum; however, the variable signal intensity was only satisfactorily minimized after also raising the temperature from 25 to 37 °C, highlighting the intrinsically dynamic nature of the DC-SIGNR CRD.

Per residue ^{15}N T_1 and T_2 relaxation times were measured for the CRD in the absence (holo) and presence of 10 mM Man_5 (Fig. 7 and Table 2) to map regions of the CRD where dynamics

TABLE 2
Average relaxation parameters of holo-CRD and Man_5-bound CRD

	Holo-CRD	Man_5-bound CRD
Average T_1 (ms)	788.26 ± 22.4	806.22 ± 40.35
Average T_2 (ms)	76.27 ± 2.27	66.54 ± 8.23
Average T_1/T_2	10.67 ± 0.43	13.19 ± 1.75
Rotational correlation time (τ_c) (ns)	10.4 ± 0.4	12.5 ± 1.36

is altered upon ligand binding. Man_5 was selected for this study because binding of $Man_9GlcNAc$ produced severely exchange-broadened spectra, preventing accurate measurement of relaxation parameters. The T_1 data are very similar for the holo-state and Man_5-bound state, showing a similar trend across the protein, and average values of 788.26 ± 22.4 ms (holo) and 806.22 ± 40.35 ms (Man_5-bound). Larger differences were observed in the transverse relaxation time constants (T_2). For the holo-CRD, although most of the T_2 values fall near the average (76.27 ± 2.27 ms), residues in both Ca^{2+} binding loops, in β-sheets 6 and 7, and at the N terminus (see *shaded regions* in Fig. 7) display significantly shorter T_2 relaxation times, suggesting that these regions are undergoing motions on the micro- to millisecond time scale due to conformational exchange processes (51). A similar trend is seen in the T_2 data for the Man_5-bound CRD but with a slightly lower average T_2 (66.54 ± 8.23 ms) and more pronounced reduction of T_2 values for the *shaded regions* in Fig. 7. These data suggest that micro- to millisecond motions present in the holo-form of the CRD still persist upon glycan binding, albeit at a slightly increased rate.

The *asterisks* in Fig. 7 indicate residues in the Ca^{2+} binding loops whose signals are so severely broadened as to be unobservable in these experiments, supporting the rapid relaxation of these regions. Specifically, these residues included Glu-359, Asn-361, and Asn-362 in the primary Ca^{2+} binding loop, which make up the EPN motif conserved among all mannose-binding C-type lectins (52). This binding at the primary Ca^{2+} site is well characterized (it is a distinguishing feature of C-type lectin binding), and it has been confirmed that the EPN sequence is responsible for mannose specificity (52). In addition to the EPN motif, residues across the entire primary Ca^{2+} binding loop and β-sheets 6 and 7 display enhanced transverse relaxation in both the holo-form and ligand-bound form. For the holo-form, the increased exchange contribution is possibly driven by the kinetics of Ca^{2+} binding, confirming that these regions are near the calcium binding sites. A further reduction in T_2 values of residues in the primary calcium binding loop are observed upon the addition of Man_5. Because there is little change in the average T_2 value between holo-form and Man_5-bound form, this enhanced relaxation is probably due to an increased conformational exchange contribution as a result of Man_5 binding kinetics or hindered motions as a result of Man_5 interacting with the principal binding site. This supports previous reports that this is the site of key CRD-mannose interactions. Interestingly, no dynamics changes were observed for residues in α-helix 2 (thought to form the extended glycan-binding "shelf") upon the addition of Man_5.

The relaxation data presented here also highlighted new regions in the CRD that have not yet been implicated in binding to sugars, namely the secondary calcium binding loop and α-helix 1. Residues all along the length of α-helix 1 show a subtle but significant reduction in T_2 (as compared with the average) in the holo-CRD and a further reduction upon binding of Man_5. α-Helix 1 is positioned toward the N terminus of the CRD, where we also see increased transverse relaxation rates for residues 269–272. The secondary calcium binding site also responds to glycan binding, despite the fact that this region has not (to our knowledge) been implicated in glycan binding previously. In the holoprotein, the reduced T_2 values in this region (Thr-337 was broadened beyond detection) were attributed to slow internal motions of the loop (on the micro- to millisecond time scale) upon binding of Ca^{2+}. The further enhancement in transverse relaxation rates upon ligand binding is less obvious because this region of the CRD has not been shown previously to form part of the extended glycan binding site.

The average T_2 value decreased significantly from 76.27 to 66.54 ms upon ligand binding. We have attributed this reduction in T_2 to slower tumbling of the ligand-bound protein compared with the holoprotein in solution. This was confirmed by using the T_1/T_2 ratio (Fig. 7) to estimate the overall rotational correlation time (τ_c) by first excluding residues that contained values more than one S.D. from the average (and thus experience a significant contribution from either chemical exchange or internal motion (53)) and then calculating as described (54). A value for the relaxation-derived τ_c of 10.4 ± 0.4 ns was obtained for the holo-CRD, which is only slightly longer than the expected value of 8.55 ns obtained using the general rule of 0.5 ns τ_c per 1 kDa of molecular mass (53–55). This deviation from the ideal value is not large enough to infer oligomerization of the CRD, but it may reflect a non-spherical shape of the monomeric protein. There is a ~17% increase in the rotational correlation time from 10.4 to 12.5 ns upon binding of Man_5 to the CRD (Table 2). Although we acknowledge that a small (~2% as estimated using a published model (56)) increase in solution viscosity upon the addition of 10 mM Man_5 may contribute to this change, and the additional size imparted by the bound sugar may also yield a very small increase, these two factors are unlikely to fully account for the increase in rotational correlation time. Likewise, binding-induced aggregation would result in a much larger increase in τ_c, suggesting that the CRD adopts a more "open" conformation as a result of Man_5 binding.

In broad terms, comparison of the relaxation and chemical shift perturbation data demonstrate that, although several regions in the CRD display micro- to millisecond time scale dynamics that persist upon glycan binding, many more residues display chemical shift perturbations. This suggests that there is a ligand-induced conformational change in the CRD. The extent of this conformational change warrants further investigation because thus far, no conformational changes have been observed in any published crystal structures for DC-SIGNR CRD upon ligand binding.

DISCUSSION

Complex carbohydrate binding events that occur within the human immune system are vital to healthy immune function and proper host responses to a wide variety of pathogens. Greater understanding of this essential glycoimmunology promises to provide important insights into major world health risks, such as HIV, tuberculosis, and Gram-negative multiresistance diseases. C-type lectins represent some of the most important receptors for complex carbohydrates, and their roles in contributing to sophisticated pathogen recognition and cellular response mechanisms are only just beginning to emerge. Structural studies have provided insights into the mechanisms via which C-type lectins assemble and bind to their targets with specificity, displaying a range of strategies, including oligomer-

ization, monosaccharide selectivity, and, in some cases, extended binding sites incorporating multiple protein-glycan contacts. However, characterization of the interaction of larger, disease-associated glycans with C-type lectins (especially HIV-derived $Man_9GlcNAc$ with the human C-type lectin DC-SIGNR) has not been reported thus far.

Here we have described the first solution state NMR backbone assignment of the carbohydrate recognition domain of human DC-SIGNR and have used this spectrum as a platform upon which to characterize the solution state binding properties of a variety of glycan ligands, including $Man_9GlcNAc$. We have also used solution NMR methods to begin to characterize the molecular dynamics of the CRD in its free and ligand-bound states for the first time. These data have revealed several interesting properties of the DC-SIGNR CRD summarized below.

Different Binding Modes and Affinities for Small Glycans versus $Man_9GlcNAc$—The C-type lectin family of proteins is striking in that substantial portions of the C-type lectin domain do not adopt regular secondary structure, and typically the ligand binding properties of the C-type lectin domains are located within these nonregular regions. Furthermore, it has been shown that a number of transmembrane human C-type lectins are capable of binding multiple ligands via discrete binding sites and can transduce different intracellular signals through the same receptor molecule, depending upon the type of ligand engaged at the extracellular face (57, 58). Another key feature of the C-type lectin family is its enormous potential for ligand binding diversity, brought about largely through the ability of the C-type lectin domain scaffold to accommodate a substantial variety of nonregular polypeptide loops at several distinct regions within the domain fold (59). It is very likely that, for these regions, the C-type lectin family has evolved into a range of homologous proteins with a very broad spectrum of ligand specificities, including targets of both exogenous and endogenous origin.

The different binding modes for the four glycans studied here, as indicated by four unique patterns of chemical shift perturbations, support the structural plasticity proposed for C-type lectins, which allows them to accommodate a wide range of diverse ligands and heterogeneously glycosylated surfaces (60). All four glycans caused perturbation of protein regions near the principal glycan binding site, namely the primary Ca^{2+}-binding loop and β-sheets 6 and 7. However, each glycan had a unique set of additional perturbations in α-helices 1 and 2, the N terminus of the CRD, the loop region consisting of residues 382–385, and the secondary Ca^{2+}-binding loop. For example, the majority of residues in α-helix 2 were preferentially engaged during binding of $(GlcNAc)_2Man_3$ (*circled* in Fig. 5*A*), which supported its role as a critical region (along with Phe-325) in forming a "shelf" complementary to $(GlcNAc)_2Man_3$ in the binding site. However, this region does not appear to interact with $Man_9GlcNAc$. Overall, the data suggest that the use of small glycans as models for binding of larger, branched physiological ligands should be treated with caution and demonstrate that solution state NMR is highly accommodating, informative, and essential for the design of drug molecules that could inhibit binding of large, disease-associated carbohydrates.

The NMR data presented here also allowed us to report the first dissociation constants for direct binding of the three glycan fragments to the DC-SIGNR CRD. The three glycan fragments displayed 1:1 binding to a single binding site with similar, weak affinities. $Man_9GlcNAc$ has a higher affinity for the CRD, as indicated by severe broadening of selected NMR signals unique to this ligand, characteristic of intermediate exchange on the NMR time scale and longer lifetimes for the complex. This higher affinity may explain the fact that $Man_9GlcNAc$ (the largest of the ligands tested) yielded the smallest number of chemical shift perturbations (*i.e.* the binding site in the DC-SIGNR CRD may have evolved around this ligand and does not need to rearrange significantly in order to accommodate it).

NMR Dynamics Reveal a High Degree of Flexibility for the DC-SIGNR CRD and Suggest New Binding Regions—Although several structural analyses of mammalian C-type lectins have revealed substantial spatial information on glycan ligand binding, the level of dynamics data relating to these carbohydrate-binding proteins is surprisingly limited. Given the considerable structural diversity of C-type lectins in nature, especially within regions of nonregular secondary structure, it follows that diversity in the dynamic characteristics of these proteins may play an important role in defining ligand interactions and specificity. Previous studies on the tunicate C-type lectin TC14 have shown that the nonregular sequences in the C-type lectin domain are rigid (61). However, just as primary sequences and ligand specificity for the C-type lectin family are many and varied, so too could be the dynamic properties of the assorted domain family members.

Our data indicate that, unlike TC14, DC-SIGNR shows considerable flexibility within its nonregular sequences, and this may contribute to its ability to interact with large, flexible glycans and transduce intracellular signals. The apo-CRD appeared to be very dynamic, probably exchanging between a broad ensemble of conformations.

Binding of Ca^{2+} and Man_5 leads to enhanced transverse relaxation rates in the primary Ca^{2+}-binding loop and β-sheets 6 and 7, known sites of key CRD-mannose interactions. This rapid relaxation could suggest direct binding and thus more hindered (yet persistent) micro- to millisecond motions in these regions or an enhanced conformational/chemical exchange contribution. This exchange could be compatible with the association/dissociation kinetics of Ca^{2+} ions or Man_5, although there are no existing data in this area. *Cis-trans* isomerization about the peptide bond of the conserved proline (Pro-360) in the EPN motif (61–65) has been reported for several other C-type lectins in their apo-form, and this could also result in the conformational exchange observed in apo-DC-SIGNR CRD.

Relaxation data also highlighted Ca^{2+}- and Man_5-induced changes in the CRD distal to the proposed glycan binding site, namely in the secondary Ca^{2+}-binding loop, α-helix 1, and the N terminus (most pronounced for Asp-271). Previous studies have suggested that Ca^{2+} binding in the secondary loop is enhanced by glycan binding (43). This type of behavior could explain the reduction in T_2 as we go from holo-form to Man_5-bound form, with enhanced Ca^{2+} binding in the secondary loop (in the presence of Man_5) leading to a more stabilized loop

structure. The secondary Ca^{2+}-binding loop lies in close proximity to the proposed binding site, and given the structural plasticity proposed for C-type lectins, which allows them to accommodate a wide range of diverse ligands, it is also possible that Man_5 has a mode of binding to the DC-SIGNR CRD different from that shown for $(GlcNAc)_2Man_3$, which includes the secondary Ca^{2+} binding loop.

The N terminus of the CRD connects to the α-helical neck in the full-length protein, and others have proposed that this region forms a flexible "hinge" (43, 66, 67), allowing the CRD to sample multiple orientations with respect to the neck. Taking this into account, one tentative explanation for the enhanced relaxation in α-helix 1 and the N terminus is that binding of Ca^{2+} and Man_5 increasingly reduces the rate of conformational interconversion of this region. Such dynamic behavior may influence ligand-induced conformational changes throughout the entire DC-SIGNR molecule, including the neck and cytoplasmic region. Alternatively, ligand binding could alter the orientation of the CRD with respect to the neck, promoting multivalent binding by adjacent CRDs. Structural analyses of the human C-type lectin CLEC5A allude to similar possibilities that dynamic changes in the CRD, attributable to distal glycan binding, could contribute to the transmission of conformational information and signaling beyond the target binding site to the intracellular regions of the native polypeptide (68). In the case of DC-SIGNR, a receptor previously believed to be involved primarily in adhesion, evidence of signaling activity has been demonstrated in the context of respiratory syncytial virus glycoprotein binding (9).

Although dynamics data could not be acquired in the case of $Man_9GlcNAc$, binding of this glycan was unique in that NMR spectra displayed severe line broadening, which could be due to extensive micro- to millisecond dynamics in the CRD (compared with Man_5-associated CRD). It follows that the larger, higher affinity $Man_9GlcNAc$ could restrict the motions of the CRD more than the smaller, low affinity Man_5; however, more work is needed to improve the solution behavior of this complex.

Together, the dynamics and chemical shift perturbation data suggest that more residues are affected by ligand binding than can be explained by direct interaction of the protein with the oligosaccharides. Our interpretation of these data leads us to portray the DC-SIGNR CRD as a highly flexible, dynamic domain that can interconvert between a number of conformations over a range of time scales. However, the crystal structures for free and ligand-bound DC-SIGNR CRD (Fig. 1*A*) do not suggest conformational rearrangement upon ligand binding. Future work will involve solving the solution structures of the holo-state and ligand-bound state in an effort to characterize these conformational changes. An alternative interpretation is that glycans bind to multiple binding sites or experience multivalent binding. For the homologous protein DC-SIGN, crystallography has revealed multiple binding modes for the smaller glycans Man_2 and Man_6. However, only a single binding mode was observed in crystals of $(GlcNAc)_2Man_3$ with DC-SIGNR, and no non-linear chemical shift perturbations or broadening (which would result from multiple binding sites and/or modes) was observed after the addition of the three sugar fragments. The linear chemical shift perturbations also fit very well to a one-site binding model. $Man_9GlcNAc$ binding did result in broadening of signals; therefore, we cannot rule out multiple binding modes for this ligand, but taken together with the rest of the data, we conclude that significant changes (both dynamic and structural) are taking place in the CRD as a result of ligand binding in solution that cannot be sampled in the crystal structures. This inherent flexibility may enhance the ability of DC-SIGNR to accommodate a variety of ligands, including those of the HIV envelope.

Acknowledgments—We thank Prof. M. Overduin (Henry Wellcome Building for Biomolecular NMR Spectroscopy, University of Birmingham) and Dr. I. Prokes (Warwick Chemistry) for NMR assistance, Dr. R. Wallis for mannose-Sepharose columns, Snezana Vasiljevic and Camille Bonomelli (University of Oxford) for technical assistance, and Dr. C. Scanlan for guidance on glycan preparation.

REFERENCES

1. Weis, W. I., Taylor, M. E., and Drickamer, K. (1998) The C-type lectin superfamily in the immune system. *Immunol. Rev.* **163,** 19–34
2. Drickamer, K. (1997) Making a fitting choice. Common aspects of sugar-binding sites in plant and animal lectins. *Structure* **5,** 465–468
3. Drickamer, K. (1999) C-type lectin-like domains. *Curr. Opin. Struct. Biol.* **9,** 585–590
4. Feinberg, H., Mitchell, D. A., Drickamer, K., and Weis, W. I. (2001) Structural basis for selective recognition of oligosaccharides by DC-SIGN and DC-SIGNR. *Science* **294,** 2163–2166
5. Soilleux, E. J., Barten, R., and Trowsdale, J. (2000) DC-SIGN; a related gene, DC-SIGNR; and CD23 form a cluster on 19p13. *J. Immunol.* **165,** 2937–2942
6. Chen, Y., Chan, V. S., Zheng, B., Chan, K. Y., Xu, X., To, L. Y., Huang, F. P., Khoo, U. S., and Lin, C. L. (2007) A novel subset of putative stem/progenitor CD34+Oct-4+ cells is the major target for SARS coronavirus in human lung. *J. Exp. Med.* **204,** 2529–2536
7. Boily-Larouche, G., Iscache, A. L., Zijenah, L. S., Humphrey, J. H., Mouland, A. J., Ward, B. J., and Roger, M. (2009) Functional genetic variants in DC-SIGNR are associated with mother-to-child transmission of HIV-1. *PLoS One* **4,** e7211
8. Chan, V. S., Chan, K. Y., Chen, Y., Poon, L. L., Cheung, A. N., Zheng, B., Chan, K. H., Mak, W., Ngan, H. Y., Xu, X., Screaton, G., Tam, P. K., Austyn, J. M., Chan, L. C., Yip, S. P., Peiris, M., Khoo, U. S., and Lin, C. L. (2006) Homozygous L-SIGN (CLEC4M) plays a protective role in SARS coronavirus infection. *Nat. Genet.* **38,** 38–46
9. Johnson, T. R., McLellan, J. S., and Graham, B. S. (2012) Respiratory syncytial virus glycoprotein G interacts with DC-SIGN and L-SIGN to activate ERK1 and ERK2. *J. Virol.* **86,** 1339–1347
10. Londrigan, S. L., Turville, S. G., Tate, M. D., Deng, Y. M., Brooks, A. G., and Reading, P. C. (2011) *N*-Linked glycosylation facilitates sialic acid-independent attachment and entry of influenza A viruses into cells expressing DC-SIGN or L-SIGN. *J. Virol.* **85,** 2990–3000
11. Dejnirattisai, W., Webb, A. I., Chan, V., Jumnainsong, A., Davidson, A., Mongkolsapaya, J., and Screaton, G. (2011) Lectin switching during dengue virus infection. *J. Infect. Dis.* **203,** 1775–1783
12. Mari, S., Serrano-Gómez, D., Cañada, F. J., Corbí, A. L., and Jiménez-Barbera, J. (2004) 1D saturation transfer difference NMR experiments on living cells. The DC-SIGN/oligomannose interaction. *Angew Chem. Int. Ed. Engl.* **44,** 296–298
13. Reina, J. J., Sattin, S., Invernizzi, D., Mari, S., Martínez-Prats, L., Tabarani, G., Fieschi, F., Delgado, R., Nieto, P. M., Rojo, J., and Bernardi, A. (2007) 1,2-Mannobioside mimic. Synthesis, DC-SIGN interaction by NMR and docking, and antiviral activity. *Chemmedchem* **2,** 1030–1036
14. Angulo, J., Díaz, I., Reina, J. J., Tabarani, G., Fieschi, F., Rojo, J., and Nieto, P. M. (2008) Saturation transfer difference (STD) NMR spectroscopy

characterization of dual binding mode of a mannose disaccharide to DC-SIGN. *Chembiochem* **9,** 2225–2227
15. Reina, J. J., Díaz, I., Nieto, P. M., Campillo, N. E., Páez, J. A., Tabarani, G., Fieschi, F., and Rojo, J. (2008) Docking, synthesis, and NMR studies of mannosyl trisaccharide ligands for DC-SIGN lectin. *Org Biomol. Chem* **6,** 2743–2754
16. Timpano, G., Tabarani, G., Anderluh, M., Invernizzi, D., Vasile, F., Potenza, D., Nieto, P. M., Rojo, J., Fieschi, F., and Bernardi, A. (2008) Synthesis of novel DC-SIGN ligands with an α-fucosylamide anchor. *Chembiochem* **9,** 1921–1930
17. Guzzi, C., Angulo, J., Doro, F., Reina, J. J., Thépaut, M., Fieschi, F., Bernardi, A., Rojo, J., and Nieto, P. M. (2011) Insights into molecular recognition of Lewis(X) mimics by DC-SIGN using NMR and molecular modelling. *Org Biomol. Chem.* **9,** 7705–7712
18. Prost, L. R., Grim, J. C., Tonelli, M., and Kiessling, L. L. (2012) Noncarbohydrate glycomimetics and glycoprotein surrogates as DC-SIGN antagonists and agonists. *ACS Chem. Biol.* **7,** 1603–1608
19. Guo, Y., Feinberg, H., Conroy, E., Mitchell, D. A., Alvarez, R., Blixt, O., Taylor, M. E., Weis, W. I., and Drickamer, K. (2004) Structural basis for distinct ligand-binding and targeting properties of the receptors DC-SIGN and DC-SIGNR. *Nat. Struct. Mol. Biol.* **11,** 591–598
20. Feinberg, H., Castelli, R., Drickamer, K., Seeberger, P. H., and Weis, W. I. (2007) Multiple modes of binding enhance the affinity of DC-SIGN for high mannose *N*-linked glycans found on viral glycoproteins. *J. Biol. Chem.* **282,** 4202–4209
21. Mitchell, D. A., Fadden, A. J., and Drickamer, K. (2001) A novel mechanism of carbohydrate recognition by the C-type lectins DC-SIGN and DC-SIGNR. Subunit organization and binding to multivalent ligands. *J. Biol. Chem.* **276,** 28939–28945
22. Sambrook, J., and Russell, D. W. (2001) Molecular Cloning: A Laboratory Manual, 3rd Ed., Cold Spring Harbor Laboratory, Cold Spring Harbor, NY
23. Dunlop, D. C., Bonomelli, C., Mansab, F., Vasiljevic, S., Doores, K. J., Wormald, M. R., Palma, A. S., Feizi, T., Harvey, D. J., Dwek, R. A., Crispin, M., Scanlan, C. N. (2010) Polysaccharide mimicry of the epitope of the broadly neutralizing anti-HIV antibody, 2G12, induces enhanced antibody responses to self oligomannose glycans. *Glycobiology* **20,** 812–823
24. Wishart, D. S., Bigam, C. G., Yao, J., Abildgaard, F., Dyson, H. J., Oldfield, E., Markley, J. L., and Sykes, B. D. (1995) H-1, C-13 and N-15 chemical-chift referencing in biomolecular NMR. *J. Biomol. NMR* **6,** 135–140
25. Liu, M. L., Mao, X. A., Ye, C. H., Huang, H., Nicholson, J. K., and Lindon, J. C. (1998) Improved WATERGATE pulse sequences for solvent suppression in NMR spectroscopy. *J. Magn. Reson.* **132,** 125–129
26. Davis, A. L., Keeler, J., Laue, E. D., and Moskau, D. (1992) Experiments for recording pure-absorption heteronuclear correlation spectra using pulsed field gradients. *J. Magn. Reson.* **98,** 207–216
27. Grzesiek, S., and Bax, A. (1992) An efficient experiment for sequential backbone assignment of medium-sized isotopically enriched proteins. *J. Magn. Reson.* **99,** 201–207
28. Wittekind, M., and Mueller, L. (1993) HNCACB, a high-sensitivity 3D NMR experiment to correlate amide-proton and nitrogen resonances with the α-carbon and β-carbon resonances in proteins. *J. Magn. Reson. Ser. B.* **101,** 201–205
29. Kay, L. E., Ikura, M., Tschudin, R., and Bax, A. (1990) 3-Dimensional triple-resonance NMR-spectroscopy of isotopically enriched proteins. *J. Magn. Reson.* **89,** 496–514
30. Bax, A., and Ikura, M. (1991) An efficient 3D NMR technique for correlating the proton and ^{15}N backbone amide resonances with the α-carbon of the preceding residue in uniformly ^{15}N/^{13}C enriched proteins. *J. Biomol. NMR* **1,** 99–104
31. Clubb, R. T., Thanabal, V., and Wagner, G. (1992) A constant-time 3-dimensional triple-resonance pulse scheme to correlate intraresidue H-1(N), N-15, and C-13′ chemical-shifts in N-15-C-13-labeled proteins. *J. Magn. Reson.* **97,** 213–217
32. Fogh, R., Ionides, J., Ulrich, E., Boucher, W., Vranken, W., Linge, J. P., Habeck, M., Rieping, W., Bhat, T. N., Westbrook, J., Henrick, K., Gilliland, G., Berman, H., Thornton, J., Nilges, M., Markley, J., and Laue, E. (2002) The CCPN project. An interim report on a data model for the NMR community. *Nat. Struct. Biol.* **9,** 416–418
33. Vranken, W. F., Boucher, W., Stevens, T. J., Fogh, R. H., Pajon, A., Llinas, M., Ulrich, E. L., Markley, J. L., Ionides, J., and Laue, E. D. (2005) The CCPN data model for NMR spectroscopy. Development of a software pipeline. *Proteins* **59,** 687–696
34. Kneller, D. G., and Goddard, T. D. (1993) *UCSF Sparky: An NMR Display, Annotation and Assignment Tool*, University of California, San Francisco
35. Shen, Y., Delaglio, F., Cornilescu, G., and Bax, A. (2009) TALOS plus. A hybrid method for predicting protein backbone torsion angles from NMR chemical shifts. *J. Biomol. NMR* **44,** 213–223
36. Schumann, F. H., Riepl, H., Maurer, T., Gronwald, W., Neidig, K. P., and Kalbitzer, H. R. (2007) Combined chemical shift changes and amino acid specific chemical shift mapping of protein-protein interactions. *J. Biomol. NMR* **39,** 275–289
37. Sudmeier, J. L., Evelhoch, J. L., and Jonsson, N. B. H. (1980) Dependence of NMR lineshape analysis upon chemical rates and mechanisms. Implications for enzyme histidine titrations. *J. Magn. Reson* **40,** 377–390
38. Fielding, L. (2007) NMR methods for the determination of protein-ligand dissociation constants. *Prog. Nucl. Magn. Reson. Spectrosc.* **51,** 219–242
39. Kay, L. E., Nicholson, L. K., Delaglio, F., Bax, A., and Torchia, D. A. (1992) Pulse sequences for removal of the effects of cross-correlation between dipolar and chemical-shift anisotropy relaxation mechanism on the measurement of heteronuclear T_1 and T_2 values in proteins. *J. Magn. Reson.* **97,** 359–375
40. Farrow, N. A., Muhandiram, R., Singer, A. U., Pascal, S. M., Kay, C. M., Gish, G., Shoelson, S. E., Pawson, T., Forman-Kay, J. D., and Kay, L. E. (1994) Backbone dynamics of a free and a phosphopeptide-complexed Src homology-2 domain studied by N-15 NMR relaxation. *Biochemistry* **33,** 5984–6003
41. Demers, J. P., and Mittermaier, A. (2009) Binding mechanism of an SH3 domain studied by NMR and ITC. *J. Am. Chem. Soc.* **131,** 4355–4367
42. Delaglio, F., Grzesiek, S., Vuister, G. W., Zhu, G., Pfeifer, J., and Bax, A. (1995) NmrPipe. A multidimensional spectral processing system based on Unix pipes. *J. Biomol. NMR* **6,** 277–293
43. Snyder, G. A., Colonna, M., and Sun, P. D. (2005) The structure of DC-SIGNR with a portion of its repeat domain lends insights to modeling of the receptor tetramer. *J. Mol. Biol.* **347,** 979–989
44. Nesmelova, I. V., Ermakova, E., Daragan, V. A., Pang, M., Menéndez, M., Lagartera, L., Solís, D., Baum, L. G., and Mayo, K. H. (2010) Lactose binding to galectin-1 modulates structural dynamics, increases conformational entropy, and occurs with apparent negative cooperativity. *J. Mol. Biol.* **397,** 1209–1230
45. Miller, M. C., Nesmelova, I. V., Platt, D., Klyosov, A., and Mayo, K. H. (2009) The carbohydrate-binding domain on galectin-1 is more extensive for a complex glycan than for simple saccharides. Implications for galectin-glycan interactions at the cell surface. *Biochem. J.* **421,** 211–221
46. Diehl, C., Engström, O., Delaine, T., Håkansson, M., Genheden, S., Modig, K., Leffler, H., Ryde, U., Nilsson, U. J., and Akke, M. (2010) Protein flexibility and conformational entropy in ligand design targeting the carbohydrate recognition domain of galectin-3. *J. Am. Chem. Soc.* **132,** 14577–14589
47. Lameignere, E., Malinovská, L., Sláviková, M., Duchaud, E., Mitchell, E. P., Varrot, A., Sedo, O., Imberty, A., and Wimmerová, M. (2008) Structural basis for mannose recognition by a lectin from opportunistic bacteria Burkholderia cenocepacia. *Biochem. J.* **411,** 307–318
48. Onizuka, T., Shimizu, H., Moriwaki, Y., Nakano, T., Kanai, S., Shimada, I., and Takahashi, H. (2012) NMR study of ligand release from asialoglycoprotein receptor under solution conditions in early endosomes. *FEBS J.* **279,** 2645–2656
49. Keeler, J. H. (2005) *Understanding NMR Spectroscopy*, John Wiley, Chichester, UK
50. Lian, L.-Y., and Roberts, G. C. K. (2011) *Protein NMR Spectroscopy: Practical Techniques and Applications*, John Wiley & Sons, Inc., New York
51. Csizmok, V., Felli, I. C., Tompa, P., Banci, L., and Bertini, I. (2008) Structural and dynamic characterization of intrinsically disordered human securin by NMR spectroscopy. *J. Am. Chem. Soc.* **130,** 16873–16879
52. Drickamer, K. (1992) Engineering galactose-binding activity into a C-type mannose-binding protein. *Nature* **360,** 183–186
53. Clore, G. M., Driscoll, P. C., Wingfield, P. T., and Gronenborn, A. M.

(1990) Analysis of the backbone dynamics of interleukin-1 β using two-dimensional inverse detected heteronuclear ^{15}N-^{1}H NMR spectroscopy. *Biochemistry* **29,** 7387–7401
54. Kay, L. E., Torchia, D. A., and Bax, A. (1989) Backbone dynamics of proteins as studied by N-15 inverse detected heteronuclear NMR-spectroscopy. Application to staphylococcal nuclease. *Biochemistry* **28,** 8972–8979
55. Copié, V., Battles, J. A., Schwab, J. M., and Torchia, D. A. (1996) Secondary structure of β-hydroxydecanoyl thiol ester dehydrase, a 39-kDa protein, derived from Hα, Cα, Cβ, and CO signal assignments and the chemical shift index. Comparison with the crystal structure. *J. Biomol. NMR* **7,** 335–340
56. Chirife, J., and Buera, M. P. (1997) A simple model for predicting the viscosity of sugar and oligosaccharide solutions. *J. Food Eng.* **33,** 221–226
57. Hibbert, R. G., Teriete, P., Grundy, G. J., Beavil, R. L., Reljic, R., Holers, V. M., Hannan, J. P., Sutton, B. J., Gould, H. J., and McDonnell, J. M. (2005) The structure of human CD23 and its interactions with IgE and CD21. *J. Exp. Med.* **202,** 751–760
58. Gringhuis, S. I., den Dunnen, J., Litjens, M., van der Vlist, M., and Geijtenbeek, T. B. (2009) Carbohydrate-specific signalling through the DC-SIGN signalosome tailors immunity to *Mycobacterium tuberculosis*, HIV-1 and *Helicobacter pylori*. *Nat. Immunol.* **10,** 1081–1088
59. Drickamer, K., and Taylor, M. E. (2005) Targeting diversity. *Nat. Struct. Mol. Biol.* **12,** 830–831
60. Bonomelli, C., Doores, K. J., Dunlop, D. C., Thaney, V., Dwek, R. A., Burton, D. R., Crispin, M., and Scanlan, C. N. (2011) The glycan shield of HIV is predominantly oligomannose independently of production system or viral clade. *PLoS ONE* **6,** e23521
61. Poget, S. F., Freund, S. M., Howard, M. J., and Bycroft, M. (2001) The ligand-binding loops in the tunicate C-type lectin TC14 are rigid. *Biochemistry* **40,** 10966–10972
62. Ng, K. K., Park-Snyder, S., and Weis, W. I. (1998) Ca^{2+}-dependent structural changes in C-type mannose-binding proteins. *Biochemistry* **37,** 17965–17976
63. Pavlícek, J., Sopko, B., Ettrich, R., Kopecký, V., Jr., Baumruk, V., Man, P., Havlícek, V., Vrbacký, M., Martínková, L., Kren, V., Pospísil, M., and Bezouska, K. (2003) Molecular characterization of binding of calcium and carbohydrates by an early activation antigen of lymphocytes CD69. *Biochemistry* **42,** 9295–9306
64. Nielbo, S., Thomsen, J. K., Graversen, J. H., Jensen, P. H., Etzerodt, M., Poulsen, F. M., and Thøgersen, H. C. (2004) Structure of the plasminogen kringle 4 binding calcium-free form of the C-type lectin-like domain of tetranectin. *Biochemistry* **43,** 8636–8643
65. Ho, M. R., Lou, Y. C., Wei, S. Y., Luo, S. C., Lin, W. C., Lyu, P. C., and Chen, C. (2010) Human RegIV protein adopts a typical C-type lectin fold but binds mannan with two calcium-independent sites. *J. Mol. Biol.* **402,** 682–695
66. Yu, Q. D., Oldring, A. P., Powlesland, A. S., Tso, C. K., Yang, C., Drickamer, K., and Taylor, M. E. (2009) Autonomous tetramerization domains in the glycan-binding receptors DC-SIGN and DC-SIGNR. *J. Mol. Biol.* **387,** 1075–1080
67. Leckband, D. E., Menon, S., Rosenberg, K., Graham, S. A., Taylor, M. E., and Drickamer, K. (2011) Geometry and adhesion of extracellular domains of DC-SIGNR neck length variants analyzed by force-distance measurements. *Biochemistry* **50,** 6125–6132
68. Watson, A. A., Lebedev, A. A., Hall, B. A., Fenton-May, A. E., Vagin, A. A., Dejnirattisai, W., Felce, J., Mongkolsapaya, J., Palma, A. S., Liu, Y., Feizi, T., Screaton, G. R., Murshudov, G. N., and O'Callaghan, C. A. (2011) Structural flexibility of the macrophage dengue virus receptor CLEC5A. Implications for ligand binding and signaling. *J. Biol. Chem.* **286,** 24208–24218